Video Article

Measuring and Mapping Patterns of Soil Erosion and Deposition Related to Soil Carbonate Concentrations Under Agricultural Management

Robert H. Erskine[1], Lucretia A. Sherrod[1], Timothy R. Green[1]

[1]Water Management and System Research Unit, Center for Agricultural Resources Research, USDA Agricultural Research Service (ARS)

Correspondence to: Robert H. Erskine at Rob.Erskine@ars.usda.gov

URL: https://www.jove.com/video/56064
DOI: doi:10.3791/56064

Keywords: Environmental Sciences, Issue 127, digital elevation model, inorganic carbon, global positioning system, geographic information systems, pedology, modified pressure-calcimeter method, soil erosion

Date Published: 9/12/2017

Citation: Erskine, R.H., Sherrod, L.A., Green, T.R. Measuring and Mapping Patterns of Soil Erosion and Deposition Related to Soil Carbonate Concentrations Under Agricultural Management. *J. Vis. Exp.* (127), e56064, doi:10.3791/56064 (2017).

Abstract

Spatial patterns of soil erosion and deposition can be inferred from differences in ground elevation mapped at appropriate time increments. Such changes in elevation are related to changes in near-surface soil carbonate ($CaCO_3$) profiles. The objective is to describe a simple conceptual model and detailed protocol for repeatable field and laboratory measurements of these quantities. Here, accurate elevation is measured using a ground-based differential global positioning system (GPS); other data acquisition methods could be applied to the same basic method. Soil samples are collected from prescribed depth intervals and analyzed in the lab using an efficient and precise modified pressure-calcimeter method for quantitative analysis of inorganic carbon concentration. Standard statistical methods are applied to point data, and representative results show significant correlations between changes in soil surface layer $CaCO_3$ and changes in elevation consistent with the conceptual model; $CaCO_3$ generally decreased in depositional areas and increased in erosional areas. Maps are derived from point measurements of elevation and soil $CaCO_3$ to aid analyses. A map of erosional and depositional patterns at the study site, a rain-fed winter wheat field cropped in alternating wheat-fallow strips, shows the interacting effects of water and wind erosion affected by management and topography. Alternative sampling methods and depth intervals are discussed and recommended for future work relating soil erosion and deposition to soil $CaCO_3$.

Video Link

The video component of this article can be found at https://www.jove.com/video/56064/

Introduction

Soil erosion threatens the sustainability of agricultural lands. Crop management, such as a conventionally-tilled winter wheat-fallow crop rotation, can accelerate erosion and deposition processes as bare soils during fallow periods are more susceptible to wind and water forces[1,2,3,4,5] (**Figure 1**). While these processes might be evident, they can be difficult to quantify.

The purpose of this study is first to provide an efficient method for quantifying and describing spatial patterns of erosion and deposition at the field scale using global positioning system (GPS) technology and geographic information systems (GIS) mapping tools. A simple conceptual model relating these patterns to near-surface soil carbonates ($CaCO_3$) is also presented and tested by prescribed field and laboratory methods. These relationships provide indirect measures of erosion and deposition, while validating the results of the GPS method. The present paper emphasizes the methods used in Sherrod *et al*. so that they can be repeated, in part or whole, for similar research in other locations[6].

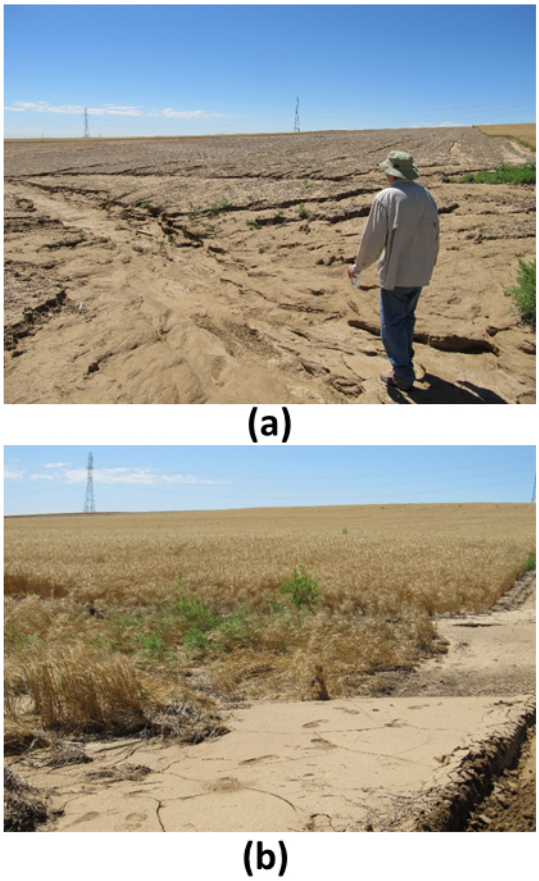

Figure 1. Photos of (a) Erosion and (b) Deposition at the Study Site Following a Heavy Rainfall Event. A tractor tire track in the lower right corner of photo (b) indicates the depth of deposition at the wheat/fallow strip border.

Various direct methods for measuring soil erosion were reviewed by Stroosnijder[7]. Suggested methods vary with the measurement purpose and resources available, but a "change in surface elevation" method is recommended at the hillslope scale and provides the advantage of measuring both erosion and deposition. One way to apply this method is to install pins in the soil and monitor the change in height of the soil relative to the top of the pin[7]. With advances in land surveying technology, however, this labor-intensive approach can be replaced by other techniques, such as terrestrial laser scanning (TLS)[8,9,10,11,12,13,14,15,16], airborne laser scanning (ALS)[17,18,19,20,21], GPS[6,22], advanced photogrammetry[23,24], or combinations of these techniques[25,26,27]. While laser scanning, commonly referred to as LiDAR (Light Detection And Ranging), provides the most rapid acquisition of dense surface elevation data sets, corrections must be made to remove standing objects, such as vegetation. With millimeter-level vertical precision, TLS can detect the smallest elevation change, however Perroy *et al*. recommended ALS over TLS for gulley erosion estimates due to the larger scanning footprint and better instrument orientation (less topographic shadowing) for scanning into deeply incised gullies[28]. Real-time kinematic GPS (RTKGPS), providing centimeter-level precision without data post-processing, is used for this study. The spatial resolution and precision of RTKGPS-collected data are optimal for detecting the dominant erosional and depositional features in an agricultural field or other environments with substantial ground cover.

The pressure-calcimeter method for quantifying soil $CaCO_3$ relies on the soil's reaction to acid in a closed system, resulting in the release of CO_2. The increase in pressure within the reaction vessel at a constant temperature is linearly correlated to the amount of soil $CaCO_3$[29]. Modifications to the traditional pressure-calcimeter method, described by Sherrod *et al*., include changing the reaction vessel to serum bottles and using a pressure transducer wired to a digital voltmeter for the detection of pressure changes[30]. These modifications allow for lower detection limits and a higher capacity for daily soil sample runs. Gravimetric or simple titrimetric methods for soil $CaCO_3$ measurement produced larger errors and detection limits than this modified pressure-calcimeter method[30].

Conceptual Model

When direct measures of erosion and deposition are not feasible, indirect indicators of these processes may be used. Sherrod *et al*. hypothesized that soil surface layer $CaCO_3$ concentration in a semi-arid climate is inversely correlated with the change in ground surface elevation (positively correlated with erosion, negatively correlated with deposition)[6]. The hypothesis should apply broadly, but specific relationships will depend upon site conditions (soil, vegetation, management, and climate). Soils at the test site (**Table 1**) typically contain a distinct calcareous layer 15-20 cm below the soil surface. Conceptually, erosion will remove the surface layer of relatively low $CaCO_3$ concentration leaving this calcareous layer of high $CaCO_3$ closer to the soil surface. The low $CaCO_3$ soil is then transported to the depositional areas, causing the calcareous layer to be buried deeper below the soil surface (**Figure 2**). Sampling these soils over time at appropriate depth intervals, either erosion or deposition (or neither) may be inferred by $CaCO_3$ concentration, according to this model.

Soil Series	Slope	Taxonomic classification	Depth	pH	EC	Total N	SOC	$CaCO_3$
	%		cm	1:2	dS m^{-1}	g kg^{-1}	g kg^{-1}	g kg^{-1}
Colby loam	5-9	fine-silty, mixed, superactive, calcareous, mesic Aridic Ustorthent	0-15	8.2	0.24	0.7	6.1	69.8
			15-30	8.3	0.24	0.5	4.0	84.3
Kim sandy loam	2-5	fine-loamy, mixed, active, calcareous, mesic Ustic Torriorthent	0-15	7.8	0.26	0.8	7.0	29.8
			15-30	8.0	0.27	0.6	5.0	51.5
	5-9	fine-loamy, mixed, active, calcareous, mesic Ustic Torriorthent	0-15	8.1	0.22	0.6	5.4	26.7
			15-30	8.1	0.19	0.5	4.1	25.8
Wagonwheel loam	0-2	coarse-silty, mixed, superactive, mesic Aridic Calciustept	0-15	8.2	0.23	0.7	5.9	66.2
			15-30	8.2	0.23	0.6	3.7	98.1
	2-5	coarse-silty, mixed, superactive, mesic Aridic Calciustept	0-15	8.3	0.23	0.8	6.6	52.0
			15-30	8.4	0.26	0.7	5.4	118.3

Table 1. Soils at the Test Site. Soil mapping units and taxonomic classification, with average soil pH, electrical conductivity (EC), total N, soil organic C (SOC), and $CaCO_3$ concentrations in the 0- to 15- and 15- to 30-cm depth increments for the Scott field in 2012 (from Sherrod *et al.*)[6].

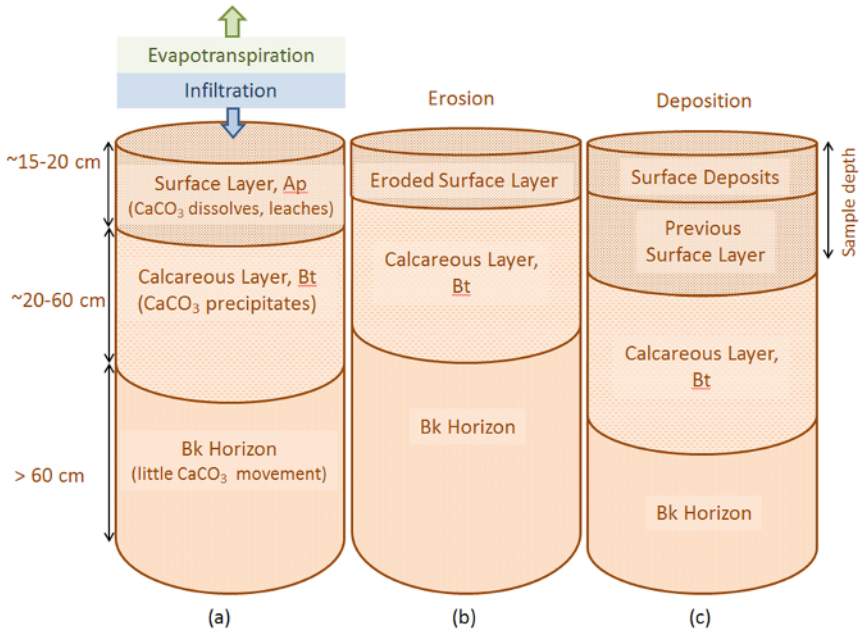

Figure 2. Conceptual Soil Profiles. Conceptual soil profiles for **(a)** a static soil matrix with $CaCO_3$ leached from the surface layer and precipitated in a deeper layer, **(b)** moderate erosion of the surface layer, and **(c)** moderate deposition of material above the previous surface layer. Depth intervals (left) are approximate based on site data (from Sherrod *et al.*)[6]. Please click here to view a larger version of this figure.

Site Description and History

The 109-ha Scott field is part of the Drake Farm in northeastern Colorado (40.61°N, 104.84°W, **Figure 3**) and was monitored from 2001 to 2012 for this study. Average annual precipitation and evapotranspiration were approximately 350 and 1200 mm, respectively, in this semi-arid climate, where convective rain of short duration and high intensity were common during the summer. Elevations range from 1559 to 1588 m in this undulating terrain with distinct landscape positions: summit, sideslope north-facing (side-NF), sideslope south-facing (side-SF), and toeslope (**Figure 4b**). Alternating strips (~120 m wide) were typically managed in this rainfed winter wheat-fallow rotation such that every other strip was fallow for about 14 months out of every 24-month rotation cycle. Shallow tillage (~7 cm), typically v-blade sweeps, occurred 4 to 6 times through the fallow period for weed control. Soils at the site were classified to have a soil-loss tolerance, or *T* value, of 11 Mg ha^{-1} $year^{-1}$, where erosion rates below this *T* value are considered acceptable for continued agricultural production[4].

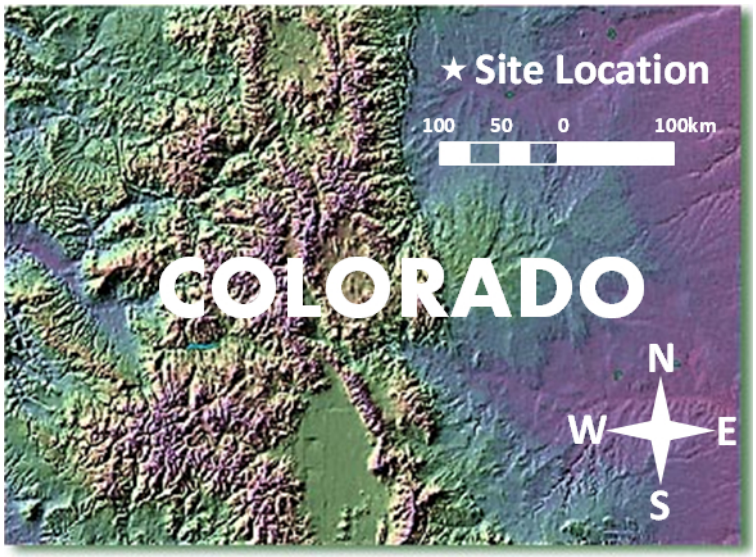

Figure 3. Site Location is Shown on a Topographic Relief Image (1011 to 4401 m) of the State of Colorado, USA. Mean elevation of the site is 1577 m.

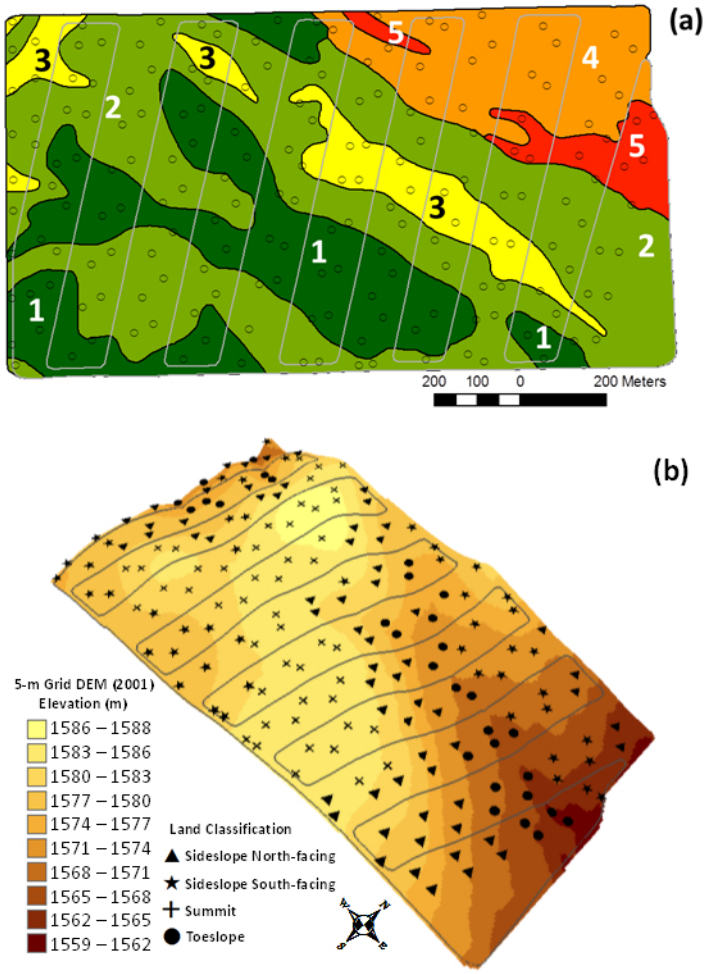

Figure 4. Soils map and Land Surface Elevation of the Scott Field. (a) Soils map of the Scott Field showing point soil sample locations and the crop management strips. Soil unit abbreviations are: 1 = Wagonwheel loam 0-2% slope, 2 = Wagonwheel loam 2-5% slope, 3 = Colby loam 5 - 9% slope, 4 = Kim fine sandy loam 2 - 5% slope, 5 = Kim fine sandy loam 5-9% slope; and **(b)** land surface elevation of the field based on the 2001 5-m grid digital elevation model (DEM), with soil sample locations shown by land classification (from Sherrod *et al.*)[6].

The first ground surface elevation survey was collected by RTKGPS in 2001 to produce a digital elevation model (DEM) for the site. In conjunction with McCutcheon *et al.*, an intensive soil sample (**Figure 4a**) was also performed in 2001, from which surface soil $CaCO_3$ were analyzed by a modified pressure-calcimeter method[30,31]. Visually evident erosion and deposition occurring over the subsequent decade due to wind, predominantly from the northwest, and rainfall-runoff events prompted a second RTKGPS elevation survey in 2009 (with a portion of the field completed in 2010). Comparison of the new DEM to the original 2001 DEM via a DEM of Difference map[32] confirmed significant erosion and deposition, displaying patterns which suggested multiple controlling factors for these processes (**Figure 5**). Given the substantial surface soil redistribution at the site and the historical soil $CaCO_3$ data, the 2001 soil sample was repeated in 2012 to test a conceptual model of hydropedological processes[6], as described in the previous section.

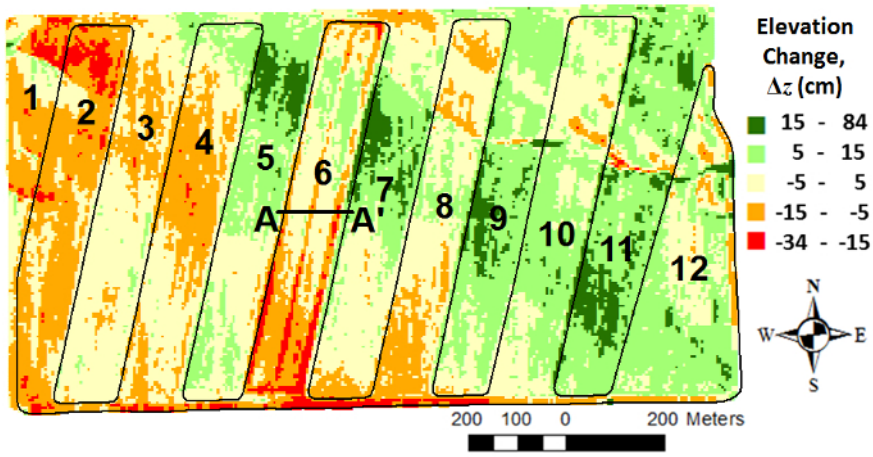

Figure 5. Map of Changes (2001-2009*) in Land Surface elevation (Δz) on a 5-m Grid within the Scott Field in Northeastern Colorado. Crop strip numbers are labeled over the alternating winter-wheat-fallow cropping system, and section A-A' is shown (details given in **Figure 11**). *Strips 2, 4, 6, 8 surveyed in 2010 to complete the 2009 DEM (from Sherrod *et al.*)[6]. Please click here to view a larger version of this figure.

Protocol

1. Land Surface Elevation Data Collection

1. GPS calibration for site
    1. Locate or set a stable benchmark in a secure location at the survey site for use as the base station GPS for RTKGPS data collection.
    2. Set up base station for RTKGPS data collection at this local benchmark using best approximation of coordinates for the base station location (*i.e.*, WAAS-corrected GPS position).
    3. With the rover GPS, visit at least three horizontal and vertical control point benchmarks within the radio communication limits of the RTKGPS (approximately 10 km radius) and record positions.
    NOTE: Benchmarks described by the National Geodetic Survey can be searched online[33] and were used here.
    4. Given the measured and published coordinates of the control points, use RTKGPS field software to perform a site calibration[34], solving for coordinates of local benchmark to be used as base station. Check that coordinate residuals (horizontal and vertical) for the control points are within tolerable limits (± 0.02 m for this calibration).

2. GPS point data collection
    1. With base station GPS set on local benchmark and using local site calibration and field software, record RTKGPS position data into GPS data collector at approximately a 5-m horizontal spacing throughout the survey area.
        1. Collect data efficiently by mounting rover GPS antenna at a measured fixed height above the ground surface on a vehicle and driving transects through the area (**Figure 6**).

    2. For vehicle method, define transect endpoints to create parallel transects spaced 5 m apart. Import transect endpoints into GPS data collector for navigation of transects while driving. Collect points with the data collector automatically once per second while driving transects at approximately 5 m s^{-1} to obtain point data about every 5 m.
    3. Repeat point data collection at site as described above at later time (8 to 9 years later in this study) so that land surface elevation changes can be analyzed; the original GPS site calibration is used for all surveys and is not repeated.

Figure 6. RTKGPS Elevation Surface Data Collection. RTKGPS elevation surface data is collected while driving a utility vehicle through the field **(a)**, while real-time GPS corrections are provided by the on-site base station **(b)**.

2. DEM Creation and Processing

1. Creating the DEMs
    1. Import position data into GIS software and interpolate to a 5-m grid DEM. Using GIS software, cross-validate measured point elevations to interpolated elevation values and choose an interpolation method that minimizes these cross-validation errors.
    NOTE: Ordinary kriging with a Gaussian semivariogram model was the optimal interpolation method for the elevation data at this site. Cross-validation also provides a measure of elevation accuracy for the survey method[35].
    2. Repeat 2.1.1 for second set of position data to create second DEM.

2. Mapping DEM change
    1. Using a raster calculator tool in GIS, subtract the most recent DEM from the original DEM to create a raster map of DEM change (**Figure 5**), where negative values of elevation change represent erosion and positive values represent deposition.

3. Land Classification
    1. Compute land surface topographic attributes (slope, aspect, contributing area) from the first grid DEM using DEM processing software.
    2. Classify land areas as summit, sideslope, or toeslope based on slope and contributing area of each DEM grid cell.
    NOTE: Summits are represented by low slopes and low contributing areas. Sideslopes are represented by high slopes and intermediate contributing areas. Toeslopes are represented by low slopes and high contributing areas. Slope and contributing area values defining these classifications will depend on the land surface topography at the site and are qualitatively chosen to give the desired representation of each classification area for a particular site.
    3. Divide sideslope areas by the two dominant aspects, north-facing and south-facing at this site.

3. Soil Sampling

1. Sample Planning
    1. Reference maps in GIS to plan soil sample locations. Choose a number of locations to adequately represent all landscape positions.
    2. Upload sample location coordinates to the GPS data collector so that sample sites can be located in the field.
    3. Use prior knowledge of soils at the site to guide decisions of sample depth increments in order to capture $CaCO_3$ variability. Pre-label sealable plastic bags to indicate sample location and depth increment.

2. Field Sampling
    1. Drive to the sample sites with a utility vehicle equipped with a hydraulic soil coring machine and the RTKGPS rover antenna for navigation.
    2. Using soil coring machine and sampling tube for desired soil core diameter (5.1 cm in this study), extract soil core from each sample location (**Figure 7**).
    NOTE: The number of cores extracted at each location, as well as the soil core depth and increments varied in this study. In 2001, a single core to a depth of 90 cm was taken and divided into 30 cm increments. In 2012, two soil cores were taken (within 1 m of the corresponding 2001 sample) to a depth of 30 cm and divided into 15 cm increments, with the two cores being aggregated for analyses. The 2012 method is recommended.
    3. Record RTKGPS position data (x, y, z) at each sample location.
    4. Cut the soil core into desired depth increments and transfer into pre-labelled sealable plastic bags and then place in coolers for transport back to the laboratory.
    5. Repeat field sampling after significant erosion and/or deposition has occurred (11 years between samples in this study).

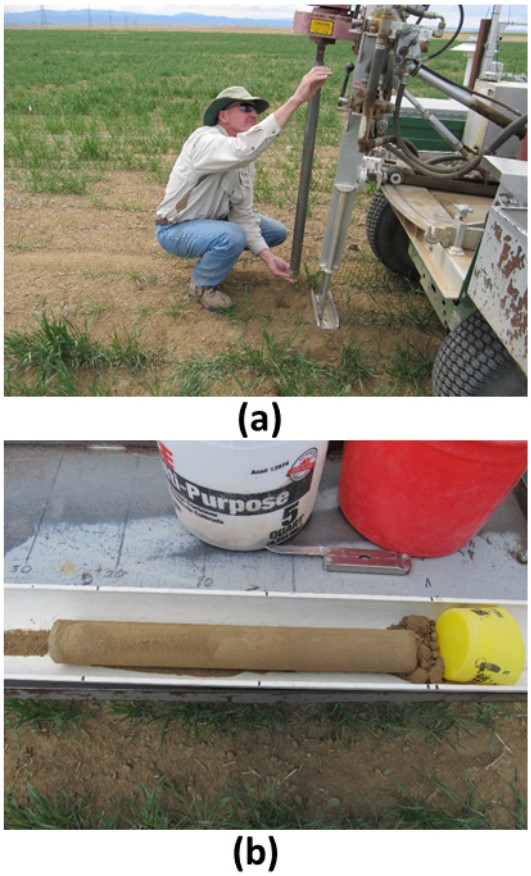

Figure 7. Soil Sampling. Soil sample locations are navigated to using a GPS-guided utility vehicle equipped with a hydraulic soil coring machine **(a)** so that soil cores can be extracted **(b)** and divided into desired depth increments.

3. Position Data Processing
    1. Measure differences in elevations recorded at each soil sample location between the two sample dates (198 locations sampled in 2001 and 2012 in this study).
    NOTE: Elevations for 2001 were taken from the 2001 DEM since point elevations were not recorded at the time of soil sampling. Positive changes in elevation > 0.05 m are considered depositional sites, while negative changes in elevation < -0.05 m are considered erosional sites.
    2. Classify each sample location as summit, North-facing sideslope, South-facing sideslope, or toeslope based on the DEM processing (see Protocol 2.3.2); classification at a single location, as defined by the slope and contributing area criteria, may be reclassified to match the dominant classification of surrounding points.
    3. Use spatial joining tools in GIS software to assign sample locations to other spatial data layers used for analyses (management strip and soil mapping unit).

4. Soils Analyses

1. Soil Sample Preparation
    1. Dry soil samples from the field at 60 °C in a laboratory oven overnight.

2. Grind oven-dried soils to pass through a 2 mm sieve using a motorized grinder or a mortar and pestle.

2. Modified Pressure-Calcimeter Apparatus Setup
    1. Set up the modified pressure-calcimeter apparatus (**Figure 8**) by connecting a pressure transducer (0 - 105 kPa range, 0.03 - 5 V DC output) to a power supply with 14 gauge wire and a digital voltmeter wired in line to monitor output from the transducer.
        1. Attach 9.5-mm ID tubing to the base of the pressure transducer and connect tubing to an 18 gauge Luer lock hypodermic needle with a particle filter (0.6 µm) in the middle to collect any reflux from reaching the pressure transducer.

    2. Use serum bottles as reaction vessels connected to the pressure transducer (**Figure 9**). Determine the size of the serum bottle to use by wetting a metal tablespoon with water and adding approximately 5 mL of soil that you expect to have high $CaCO_3$ concentration. Pipet 1 mL of 0.5 N H_2SO_4 to this soil and observe effervescence.
    3. If effervescence is high, then assume greater than 15% $CaCO_3$ concentration and use a 100 mL serum bottle as the reaction vessel, otherwise use a 20 mL serum bottle.

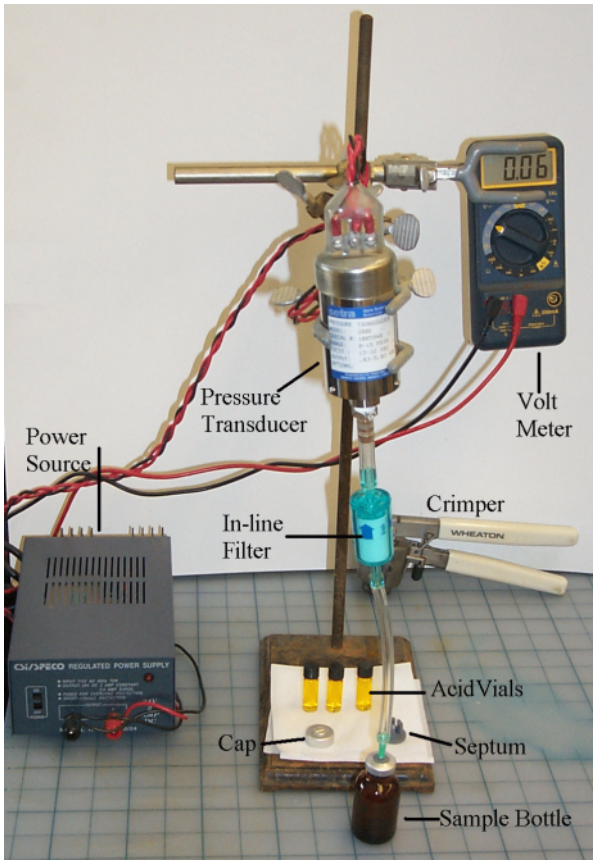

Figure 8. Modified Pressure-calcimeter Apparatus. The modified pressure-calcimeter apparatus uses a serum bottle as the reaction vessel and a pressure transducer wired to a voltage meter to output the signal (from Sherrod *et al.*)[30].

Figure 9. Reaction Vessels for the Modified Pressure-calcimeter Method. Reaction vessels for the modified pressure-calcimeter method are serum bottles containing a 0.5 dram vial with 2 mL acid reagent and a 1 g soil sample.

3. Carbonate Measurement
    1. Place a 1 g subsample of the prepared soil (see Protocol 4.1) into a labelled reaction vessel. For soils containing greater than 50% $CaCO_3$, use only 0.5 g of soil.
    2. Pipet 2 mL of acid reagent (6 N HCl containing 3% $FeCL_2O_4H_2O$) into a 0.5 g glass vial. Place vial into reaction vessel gently so that the solution contents do not spill out by tilting the reaction vessel almost to the side position.
    3. While keeping the reaction vessel containing the soil sample and acid vial tilted, seal with gray butyl rubber stoppers and crimp with aluminum sealing ring.

4. Shake reaction vessel with a swirling motion to insure complete mixing of soil with acid. Place the reaction vessel on the lab bench and let the reaction proceed for at least 2 hr.
5. While waiting for reaction vessels to complete, determine a standard curve by measuring voltages of known $CaCO_3$ concentrations using the same reaction vessel setup as soil samples (**Figure 10**). Mix 100% $CaCO_3$ with glass beads or sand on a weight percentage basis to create known $CaCO_3$ concentrations. Include a blank sample without $CaCO_3$.
6. After soil sample reactions are complete, pierce the rubber septum of the reaction vessel with an 18 gauge hypodermic needle and record voltage output by the pressure transducer.
7. Solve for $CaCO_3$ percentage given the measured voltage and the equation determined from the standard curve (**Figure 10a**).
NOTE: Increase in pressure produced by release of CO_2 is linearly related to the concentration of $CaCO_3$ present in the soil such that:
% $CaCO_3$ = (regression coefficient * change in pressure in volts) + intercept.

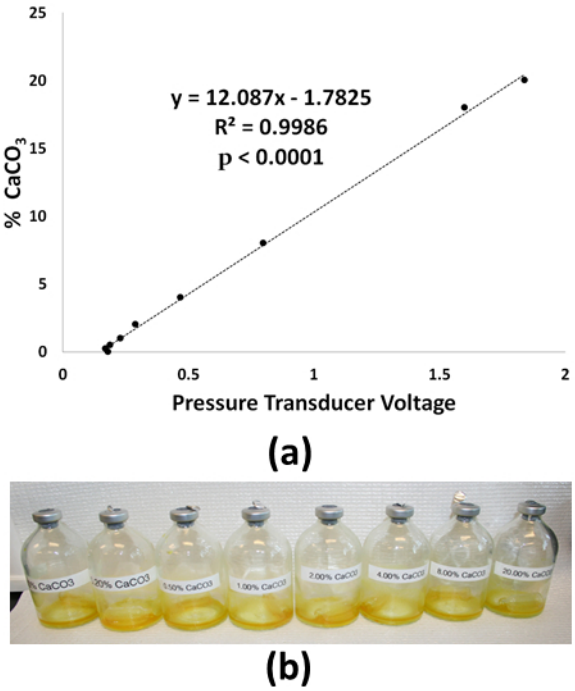

Figure 10. $CaCO_3$ Measurement. (a) A standard curve for $CaCO_3$ is created using the voltage readings from the pressure transducer based on known percentages of $CaCO_3$ **(b)** mixed with powder glass beads or sand.

5. Statistical Analyses

1. Define two dependent variables as the change in ground surface elevations and soil surface layer $CaCO_3$ concentrations from the first to second sample dates (2001 to 2012 in this study). Define independent or explanatory variables as management (odd- or even- numbered strip), individual strips, west or east block of strips, soil mapping unit, landscape classification, and erosional/depositional classification.
2. Perform correlation analysis and analysis of variance to statistically quantify relationships between variables. Perform analyses in any preferred statistical package.

Representative Results

Mapping DEM differences from 2001 and 2009 reveals erosion (red) and deposition (green) over that 8-year period, with decimeter-level changes in elevation over most areas (**Figure 5**). At the field-scale, erosion is dominant in the west and southwest, while deposition is seen along a northwest to southeast diagonal band on the eastern side of the field. Alternating bands of erosion and deposition are seen at the management-scale, often with abrupt changes at the management strip boundaries. Patterns related to soil types (**Figure 4a**) are less pronounced but do appear to coincide with topographic features with which soil types are strongly interrelated. Fine-scale erosional and depositional patterns are seen resembling water flow paths in areas of topographic convergence. Three distinct linear features of erosion, parallel to management, are seen in Strip 6. A west-east transect (**A-A'** in **Figure 5**) is plotted to examine these unique features (**Figure 11**), which were most likely caused by tillage operations. No soil sample sites were located within these features in Strip 6.

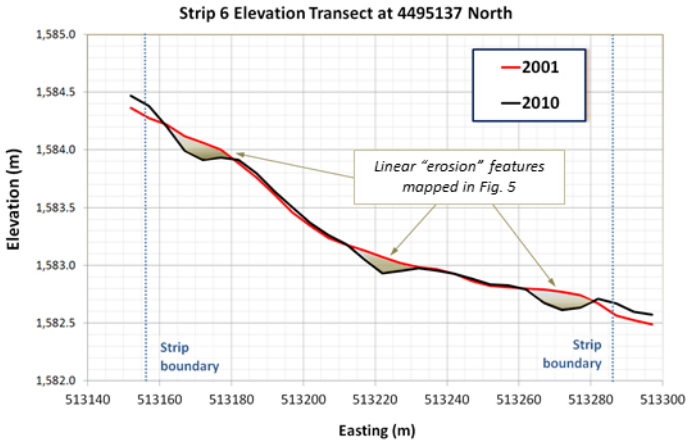

Figure 11. Elevation Profiles (2001 and 2009* DEMs) Along a West-east Transect Through Strip 6 (A-A' in Figure 5). *Strip 6 elevation data collected in 2010.

Dividing the western management strips (West Block, Strips 1 - 6, **Figure 5**), where erosion was dominant, from the eastern management (East Block, Strips 7 - 12, **Figure 5**), where deposition was dominant, an inverse relationship is shown between the change in surface soil $CaCO_3$ ($\Delta CaCO_3$) and the change in land surface elevation (Δz) at the sample sites between 2001 and 2012 (**Figure 12**). In the erosional West Block, $CaCO_3$ concentrations increased an average of approximately 3 g kg^{-1} while the average elevation decreased approximately 2 cm. Conversely, the depositional East Block showed an average > 4 g/kg decrease in $CaCO_3$ concentrations while the average elevation increased approximately 5 cm. This inverse relationship is not present when pooling all strips together over the entire field.

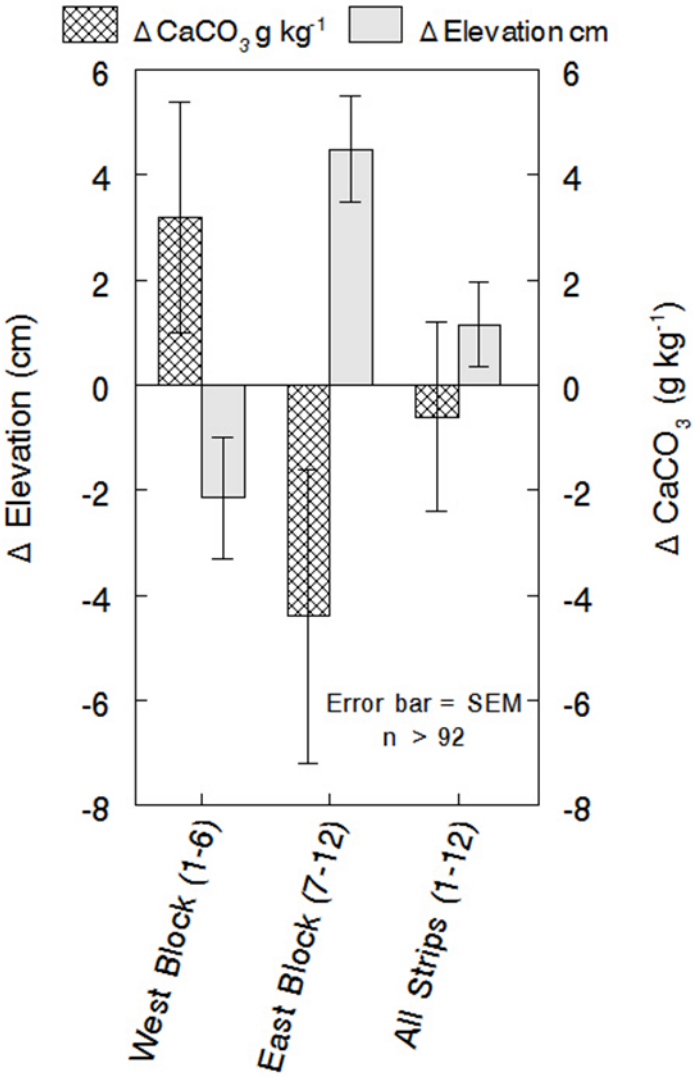

Figure 12. Spatially Averaged Change in $CaCO_3$ Concentration (0-30-cm depth) and Land Surface Elevation as Affected by Blocks of West (Strips 1-6) and East (Strips 7-12) Management Areas after 11 Years (2001-2012). Figure 5 shows strip numbers and boundaries. Error bars are ±1 SEM (from Sherrod *et al.*)[6].

Separating erosional sample locations (Δz < -5 cm) from depositional locations (Δz > 5 cm), all landscape positions reveal an inverse relationship between $\Delta CaCO_3$ and Δz, except north-facing sideslopes (**Figure 13**). Averaging across all landscapes, this inverse relationship is maintained in erosional locations; in depositional locations, however, $\Delta CaCO_3$ is nearly unchanged. For depositional locations, deposition is greatest in toeslope positions, averaging near 13 cm. Average decreases in $CaCO_3$ are also greatest (8.2 g/kg) in these depositional toeslope positions. For the erosional sample locations, average erosion is greatest (17.4 cm) at north-facing sideslopes, however, this did not correspond with an increase in $CaCO_3$ as seen in all other erosional landscape positions. Assuming a soil bulk density of 1.4 g/cm^3, a 17.4 cm soil loss equals an erosion rate of 221 Mg/ha/year over the study period, nearly 20 times the *T* value for this site. Calculation of net erosion over the entire field would require detailed knowledge of soil bulk density before erosion and after deposition. Since there is an average net gain in elevation over the field, a constant bulk density would indicate a net deposition, but since deposited soils are likely at a lower bulk density than before being transported, a net soil loss is assumed.

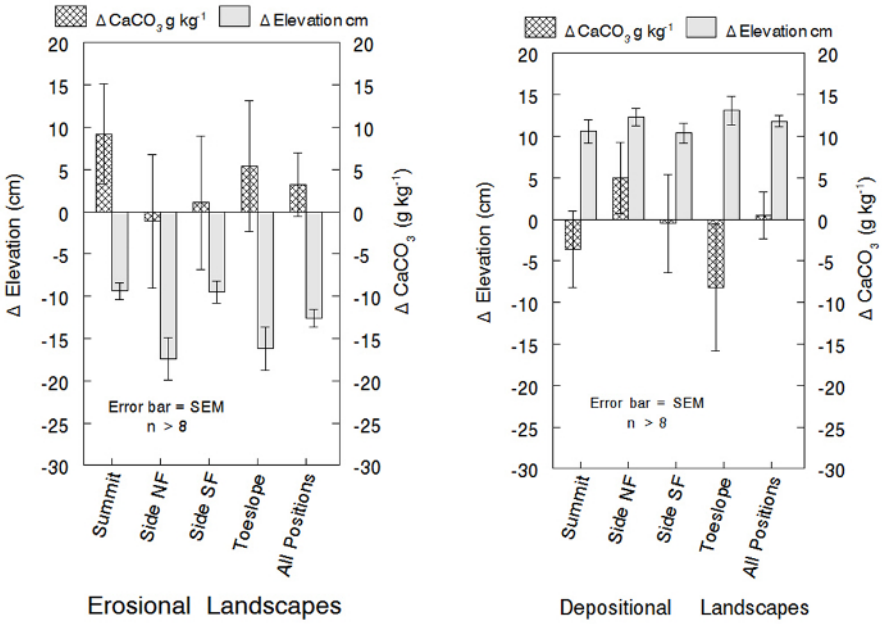

Figure 13. Spatially Averaged Change (2001-2012) in $CaCO_3$ Concentration (0-30-cm depth) and Land Surface Elevation as Affected by Landscape Classification in Erosional and Depositional Landscape Areas; NF is north facing and SF is south facing (from Sherrod *et al.*)[6]. Please click here to view a larger version of this figure.

A correlation analysis of Δz and $\Delta CaCO_3$ with site variables related to management (odd- or even- numbered strip), individual strips, west or east block of strips, soil mapping unit, and landscape position is presented in **Table 2**. The most significant correlations ($p < 0.0001$) are seen between Δz and individual management strips or strip blocks (west or east). Change in $CaCO_3$ was most significantly correlated ($p = 0.016$) to the soil mapping unit, while Δz was not correlated to soils. Less significant ($p = 0.036$) was the correlation between $\Delta CaCO_3$ and the strip blocks, with which Δz was correlated as well. An analysis of variance shows Δz to be significantly affected ($p < 0.06$) by all site variables (**Table 3**). Erosional class (erosional, depositional, or unchanged: EDU) most significantly ($p = 0.075$) affected $\Delta CaCO_3$, followed by soil mapping unit and individual strips, both significant below a 10% significance level.

			Pearson correlation coefficient			
Variable	**Strips**	**Block**	**Soil**	**Landscape**	**$\Delta CaCO_3$**	**Δz**
Management	0.090 (0.222)*	-0.027 (0.715)	0.028 (0.708)	0.004 (0.959)	0.019 (0.799)	-0.115 (0.120)
Strips	-	0.868 (<0.0001)	0.411 (<0.0001)	0.077 (0.295)	-0.120 (0.104)	0.425 (<0.0001)
Block		-	0.414 (<0.0001)	0.114 (0.124)	-0.154 (0.036)	0.303 (<0.0001)
Soil			-	0.408 (<0.0001)	-0.177 (0.016)	0.025 (0.738)
Landscape				-	-0.101 (0.172)	-0.083 (0.260)
$\Delta CaCO_3$					-	-0.001 (0.990)
* Pr > r in parentheses.						

Table 2. Correlation Analysis of Δz and $\Delta CaCO_3$ with Site Variables. Correlation matrix for site variables associated with elevation (z) and $CaCO_3$ changes after 11 years as affected by management (odd or even strips), individual strips, west block (Strips 1 - 6) or east block (Strips 7 - 12), soil mapping unit, and landscape position (summit, side-north facing, side-south facing, and toeslope) (from Sherrod *et al.*)[6].

	ΔElevation		$\Delta CaCO_3$	
Variable	**F value**	**Pr > F**	**F value**	**Pr > F**
Management	3.47	0.0643	0.07	0.7957
Strips	50.25	<0.0001	2.84	0.0937
Block	7.48	0.0069	1.79	0.1824
Soil	5.57	0.0193	3.16	0.0773
EDU	NA*	NA	3.21	0.0750
* NA, not applicable because EDU is determined from ΔElevation.				
EDU = Erosional (E), Depositional (D), Unchanged (U)				

Table 3. Analysis of Variance for Dependent Variables of Change in Elevation and Change in $CaCO_3$ Concentration. Analysis of variance for dependent variables of change in elevation and change in $CaCO_3$ concentration in the 0- to 30-cm depth increment after 11 years as affected by management (odd or even strips), individual strips, west block (Strips 1 - 6) or east block (Strips 7 - 12), soil mapping unit, and erosional class (EDU): erosional (Δz < -5 cm), depositional (Δz > 5 cm), or unchanged (-5 cm < Δz < 5 cm) (from Sherrod *et al.*)[6].

Interpolation of the surface $CaCO_3$ point samples in 2001 and 2012 results in the maps shown (**Figures 14a, 14b**), and a difference map is created from these to show interpolated $\Delta CaCO_3$ (**Figure 14c**). Relatively small, concentrated areas of high and low $CaCO_3$ seen in the 2001 map (**Figure 14a**) are no longer seen in 2012 where the spatial patterns are less complex (**Figure 14b**). This "smoothing" of the 2001 map to the 2012 map indicates an increase in $CaCO_3$ in previously lower $CaCO_3$ areas and a decrease in $CaCO_3$ where $CaCO_3$ was high. Patterns of $\Delta CaCO_3$ (**Figure 14c**) show most increases in the far west, and some relationship to the land surface topography.

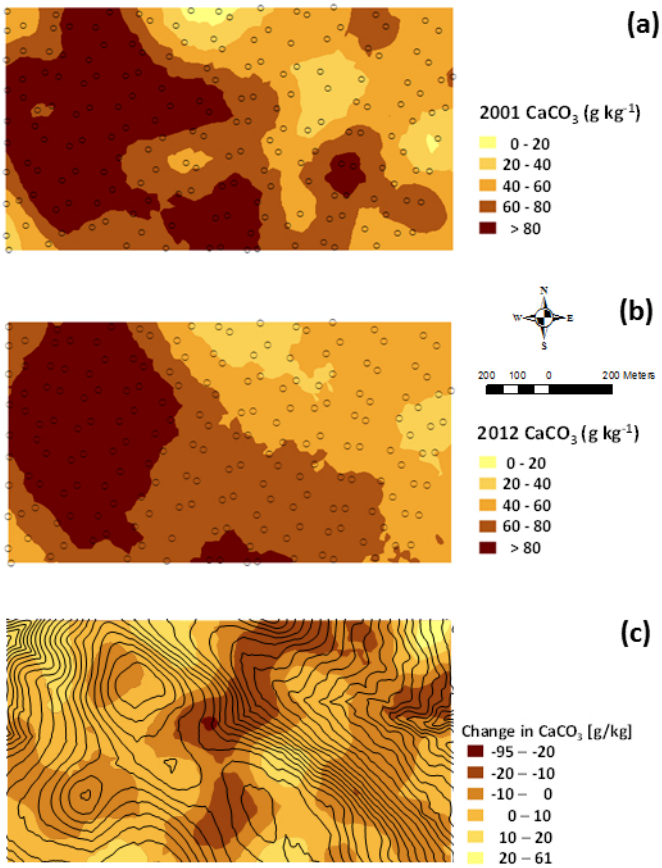

Figure 14. Kriged Interpolation Maps of $CaCO_3$ Concentrations. Kriged interpolation maps of $CaCO_3$ concentrations in the depth interval 0 to 30 cm for **(a)** 2001, **(b)** 2012, and **(c)** change from 2001 to 2012. Soil sample locations are shown by circles (a, b) and elevation contours with 1-m intervals are shown in (c) (from Sherrod *et al.*)[6].

Discussion

Mapped changes in elevation (**Figure 5**) illustrate significant erosion and deposition on an agricultural field and spatial patterns indicative of multiple controlling factors over multiple scales. From field scale patterns associated with wind, down to fine scale dendritic patterns produced by water flow, processes relevant to this study are discernable. The level of elevation change detection provided by repeated RTKGPS ground

surveys appears optimal. Finer detection levels, as provided by TLS, may complicate results by introducing microtopographic features, such as cropping ridges and furrows, while coarser detection levels, as found with airborne surveys, might not be sufficient to capture fine scale patterns. Conducting RTKGPS ground surveys over an area of this size (~100 ha) takes a few days, however, due to the limitations of collecting only a single point per second and the travel time to cover the site area. Advances in airborne surveys may provide better alternative methods in the future if survey accuracies can improve to match the accuracy of ground surveys used here.

Mixed results were seen in correlating changes in surface soil $CaCO_3$ with changes in land surface elevation, as predicted by the conceptual model. In 2001, surface soil samples for $CaCO_3$ concentrations were only available in one depth increment over the top 30 cm. In 2012, the soil samples were divided into two 15 cm increments over the top 30 cm. An analysis of $\Delta CaCO_3$ in only the top 15 cm will likely change these results and may prove to be more strongly related to erosion and deposition. The modified pressure-calcimeter method[30] continues to serve as an efficient method for soil $CaCO_3$ measurement.

This paper provides a detailed approach for field-scale quantification and description of erosional and depositional processes in an agricultural field. The methods described here can be applied to other sites where calcareous layers are present near the soil surface. Future work is planned for this site to compute a new DEM using and to measure surface elevation changes since 2009, when the last complete RTKGPS ground survey was conducted. Also, the soil sampling scheme of 2012 for surface soil $CaCO_3$ will be repeated in 15 cm depth increments so that changes in the top 15 cm can be compared between the future sample and 2012.

Disclosures

The authors have nothing to disclose.

Acknowledgements

The field study site is on a farm managed by David Drake and we thank him for his cooperation during this long-term research. We also thank Mike Murphy for his many years of field work on this project and Robin Montenieri for her help with graphics used in this paper.

References

1. Freebairn, D. M. Erosion control - some observations on the role of soil conservation structures and conservation. *Nat. Res. Mgt.* **7** (1), 8-13, (2004).
2. Garcia-Orenes, F., Roldan, A., Mataix-Solera, J., Cerda, A., Campoy, M., Arcenegui, V., Caravaca, F. Soil structural stability and erosion rates influenced by agricultural management practices in a semi-arid Mediterranean agro-ecosystem. *Soil Use and Mgt.* **28**, 571-579 (2012).
3. Hass, H. J., Willis, W. O., Bond, J. J. General relationships and conclusions. *Summer Fallow in the Western United States. USDA-ARS Conserv. Res. Rpt. No. 17*. U. S. Government Printing Office, Washington, D. C., 149-160, (1974).
4. Montgomery, D. R. Soil erosion and agricultural sustainability. *Proc. of the Nat. Acad. of Sci. of the USA*. **104** (33), 13268-13272 (2007).
5. Skidmore, E. L., Layton, J. B., Armbrust, D. V., Hooker, M. L. Soil physical properties as influenced by cropping and residue management. *Soil Sci. Soc. of Am. J.* **50** (2), 415-419, (1986).
6. Sherrod, L. A., Erskine, R. H., Green, T. R. Spatial patterns and cross-correlations of temporal changes in soil carbonates and surface elevation in a winter wheat-fallow cropping system. *Soil Sci. Soc. of Am. J.* **79** (2), 417-427 (2015).
7. Stroosnijder, L. Measurement of erosion: Is it possible? *Catena*. **64**, 162-173 (2005).
8. Dabek, P., Zmuda, R., Cmielewski, B., Szczepanski, J. Analysis of water erosion processes using terrestrial laser scanning. *Acta Geodynam. Et Geomat.* **11** (1), 45-52 (2014).
9. Day, S. S., Gran, K. B., Belmont, P., Wawrzyniec, T. Measuring bluff erosion part 1: terrestrial laser scanning methods for change detection. *Earth Surf. Proc. and Landforms.* **38** (10), 1055-1067 (2013).
10. Eltner, A., Baumgart, P. Accuracy constraints of terrestrial Lidar data for soil erosion measurement: Application to a Mediterranean field plot. *Geomorph.* **245**, 243-254 (2015).
11. Letortu, P., *et al.* Retreat rates, modalities and agents responsible for erosion along the coastal chalk cliffs of Upper Normandy: The contribution of terrestrial laser scanning. *Geomorph.* **245**, 3-14 (2015).
12. Longoni, L., *et al.* Monitoring Riverbank Erosion in Mountain Catchments Using Terrestrial Laser Scanning. *Rem. Sens.* **8** (3), 241 (2016).
13. Meijer, A. D., Heitman, J. L., White, J. G., Austin, R. E. Measuring erosion in long-term tillage plots using ground-based lidar. *Soil & Till. Res.* **126**, 1-10 (2013).
14. Rengers, F. K., Tucker, G. E., Moody, J. A., Ebel, B. A. Illuminating wildfire erosion and deposition patterns with repeat terrestrial lidar. *J. of Geophys. Res.-Earth Surf.* **121** (3), 588-608 (2016).
15. Schubert, J. E., Gallien, T. W., Majd, M. S., Sanders, B. E. Terrestrial Laser Scanning of Anthropogenic Beach Berm Erosion and Overtopping. *J. of Coast. Res.* **31** (1), 47-60 (2015).
16. Stenberg, L., *et al.* Evaluation of erosion and surface roughness in peatland forest ditches using pin meter measurements and terrestrial laser scanning. *Earth Surf. Proc. and Landforms.* **41** (10), 1299-1311 (2016).
17. Croke, J., Todd, P., Thompson, C., Watson, F., Denham, R., Khanal, G. The use of multi temporal LiDAR to assess basin-scale erosion and deposition following the catastrophic January 2011 Lockyer flood, SE Queensland, Australia. *Geomorph.* **184**, 111-126 (2013).
18. Earlie, C., Masselink, G., Russell, P., Shail, R. Sensitivity analysis of the methodology for quantifying cliff erosion using airborne LiDAR - examples from Cornwall, UK. *J. of Coast. Res. Spec. Iss.* **65**, 470-475 (2013).
19. Kessler, A. C., Gupta, S. C., Dolliver, H. A. S., Thoma, D. P. Lidar Quantification of Bank Erosion in Blue Earth County, Minnesota. *J. of Env. Quality.* **41** (1), 197-207 (2012).
20. Pye, K., Blott, S. J. Assessment of beach and dune erosion and accretion using LiDAR: Impact of the stormy 2013-14 winter and longer term trends on the Sefton Coast, UK. *Geomorph.* **266**, 146-167 (2016).

21. Thoma, D. P., Gupta, S. C., Bauer, M. E., Kirchoff, C. E. Airborne laser scanning for riverbank erosion assessment. *Rem. Sens. of Env.* **95** (4), 493-501 (2005).
22. Zhang, C. L., Yang, S., Pan, X. H., Zhang, J. Q. Estimation of farmland soil wind erosion using RTK GPS measurements and the Cs-137 technique: A case study in Kangbao County, Hebei province, northern China. *Soil & Till. Res.* **112** (2), 140-148 (2011).
23. Neugirg, F., *et al.* Erosion processes in calanchi in the Upper Orcia Valley, Southern Tuscany, Italy based on multitemporal high-resolution terrestrial LiDAR and UAV surveys. *Geomorph.* **269**, 8-22 (2016).
24. Pineux, N., *et al.* Can DEM time series produced by UAV be used to quantify diffuse erosion in an agricultural watershed? *Geomorph.* **280**, 122-136 (2017).
25. Bremer, M., Sass, O. Combining airborne and terrestrial laser scanning for quantifying erosion and deposition by a debris flow event. *Geomorph.* **138** (1), 49-60 (2012).
26. Day, S. S., Gran, K. B., Belmont, P., Wawrzyniec, T. Measuring bluff erosion part 2: pairing aerial photographs and terrestrial laser scanning to create a watershed scale sediment budget. *Earth Surf. Proc. and Landforms.* **38** (10), 1068-1082 (2013).
27. De Rose, R. C., Basher, L. R. Measurement of river bank and cliff erosion from sequential LIDAR and historical aerial photography. *Geomorph.* **126** (1-2), 132-147 (2011).
28. Perroy, R. L., Bookhagen, B., Asner, G. P., Chadwick, O. A. Comparison of gully erosion estimates using airborne and ground-based LiDAR on Santa Cruz Island, California. *Geomorph.* **118** (3-4), 288-300 (2010).
29. Loeppert, R. H., Suarez, D. L. Carbonate and Gypsum. *Methods of Soil Analysis. Part 3. Chemical Methods. 3rd ed. SSSA Book Series 5.* Sparks, D. L., *et al.* (ed.). SSSA, Madison, WI, 437-474, (1996).
30. Sherrod, L. A., Dunn, G., Peterson, G. A., Kilberg, R. L. Inorganic carbon analysis by modified pressure-calcimeter method. *Soil Sci. Soc. of Am. J.* **66** (1), 299-305, (2002).
31. McCutcheon, M. C., Farahani, H. J., Stednick, J. D., Buchleiter, G. W., Green, T. R. Effect of soil water on apparent soil electrical conductivity and texture relationships in a dryland field. *Biosyst. Eng.* **94** (1), 19-32 (2006).
32. Wheaton, J. M., Brasington, J., Darby, S. E., Sear, D. A. Accounting for uncertainty in DEMs from repeat topographic surveys: improved sediment budgets. *Earth Surf. Proc. and Landforms.* **35** (2), 136-156 (2010).
33. *https://www.ngs.noaa.gov/datasheets/.* (2017).
34. Trimble Inc. Survey - Calibration. *Trimble Access Software - General Survey. Version 1.60. Revision A.* 214-219, (2011).
35. Erskine, R. H., Green, T. R., Ramirez, J. A., MacDonald, L. H. Digital elevation accuracy and grid cell size: effects on estimated terrain attributes. *Soil Sci. Soc. of Am. J.* **71**, 1371-1380 (2007).

